Practical Implementation of Functionally Graded Lattice Structures in a Bicycle Crank Arm

Thierry DECKER, Slawomir KEDZIORA and Claude WOLF
Faculty of Science, Technology and Communication
University of Luxembourg, 6 rue Coudenhove-Kalergi
L-1359 Luxembourg City, Luxembourg

Abstract: Functionally graded lattice structures (FGLS) were studied thoroughly for the past years, mostly focusing on specific synthetic tests in the context of additive manufacturing while rarely being actually applied outside of this specific domain. This paper examines a way to practically implement them in a commonly used appliance and study their potential for its improvement. A bicycle crank arm was chosen for this purpose, and a solid aluminium reference model (Shimano FC-R450-453) is used as a performance baseline. The novel design is composed of a hollow body containing a beam-based, non-stochastic, functionally graded lattice structure and is planned to be manufactured on a Markforged Metal X system using 17-4 PH stainless steel. It aims to increase the total stiffness under EN ISO 4210-8 norm loading conditions compared to the reference model while limiting mass and stress values to acceptable degrees. Two crank arm variants, containing a face-centred cubic (FCC) and re-entrant auxetic lattice respectively, are optimised by locally altering their beam radii in eight separate regions. The displacement at the load application point is minimised using Altair OptiStruct and HyperStudy. The reference crank, weighing 213g, exhibits a deflection magnitude of 7.1mm in the most demanding load case while the newly designed and optimised versions only showed displacements of 2.52mm (FCC lattice, 340g) and 2.58mm (re-entrant lattice, 339g) respectively. In addition, the stress distribution was significantly enhanced compared to the reference model, as the latter would not pass the fatigue tests required by the norm. This demonstrates that FGLS, in combination with high-strength materials and additive manufacturing, can increase the performance of many parts, although in this case, with a trade-off in terms of its mass. In future projects, it might be considerably reduced by utilising alternative lattice types lattices or other materials while preserving the benefits of FGLS.

Keywords: Additive Manufacturing, Functionally Graded Lattice Structures, Design Exploration, Finite Element Method, Cellular Structures

1 Outline

1.1 Introduction

Additive manufacturing (AM) is being adopted rapidly across many scientific and industrial domains as it enables completely new design approaches, material blends, and manufacturing flexibility. It democratises manufacturing rendering it available to small businesses and, in the case of plastic AM machines, even to individual persons thanks to its easy accessibility and steadily decreasing costs. High-performance metals, ceramics, fiber reinforced plastics, and even biological materials fit for AM are researched heavily, gradually improving their properties and ease of use. Furthermore, novel artificial structures like cellular solids emerged mimicking light-weight, porous configurations commonly found in nature, e.g., in cancellous bone or fungi mushrooms. They can be constituted of beams or surface-based unit cells and were coined functionally graded lattice structures (FGLS) as they exhibit locally varying mechanical properties adapted to the requirements. They fall in the category of mechanical metamaterials, the behaviour of which is mostly defined by their structural layout rather than their base material. These can be tailored to exhibit specific characteristics like exceptionally high strength-to-weight ratio, energy absorption, negative Poisson's ratio [1] (in that case called auxetic structures), or negative thermal expansion coefficient [2]. Although many scientific analyses study the behaviour of FGLS and demonstrate their potential, they predominantly focus on synthetic assessments like vibration [3], impact [4], compression [5], or heat exchanging properties [6]. This situation makes reports on their implementation of real-world parts scarce, which this paper aims to remedy. Our hypothesis is that combining FGLS with high-performance materials in a common mechanical appliance can significantly improve its performance compared to a generic solid counterpart produced by conventional manufacturing means. For this purpose, a bicycle crank arm was chosen. The aim is to design a crank arm fit for use on mountain bikes with a functionally graded lattice structure core surpassing the stiffness of a conventional crank arm. It is to be optimised for maximum stiffness while limiting stress and weight values to acceptable levels. The widespread use of bicycle cranks makes them an approachable demonstrator, and their size is suitable for the AM machine at hand: a Markforged Metal X system.

1.2 State of the art

While unit cells and their composition as FGLS currently are a vibrant research topic, their properties are largely investigated in an isolated manner rather than holistically and their industrial use is still a rare occurence. Comprehensive overviews are provided in [2], [7] and [8]. Custom-written code or elaborate, manual CAD operations are often used to generate specific lattices since only few software suites exist to handle the needs of researchers and engineers alike, mostly offering a limited number of options to manipulate lattice properties [7]. Relevant software suites like Autodesk Netfabb or Ansys SpaceClaim mainly offer basic lattice creation and modification tools with optional local density grading capabilities. A novel, more advanced approach is pursued by nTopology Platform providing significant advantages in terms of its lattice manipulation capabilities, ease of use and design iteration speed [9]. Industrial case studies show potential for improvement in performance and weight in various applications (see [10], [11], [12] and others). Lattice structures in additively manufactured parts also start to be applied in bicycling appliances. Some examples include polymer saddles [13], titanium crank arms with varying wall thicknesses [14], or frames consisting of steel or titanium lugs combined with carbon fiber reinforced polymer tubes [15]. The lattices used in these cases appear to be uniform in nature rather than functionally graded.

2 Materials and Procedure

2.1 Materials

Inexpensively produced bicycle crank arms are commonly forged using 6061-T6 aluminium, as is assumed to be the case with the chosen Shimano crank model. The new crank design containing the lattice will, in a first iteration, be made of 17-4 PH stainless steel available for the Markforged Metal X system at hand. This choice was made as it was the only complete property dataset available for base materials provided by Markforged. Aluminium or titanium would have been the preferred material for this endeavour, but are not yet available for the Markforged Metal X system. The mechanical properties of 17-4 PH SS manufactured via SLM have been investigated thoroughly (see [16], [17]); however, at the time of writing and to the authors' knowledge, no independent studies confirming the material data provided by Markforged seem to be publicly available. Table 1 specifies the material properties used hereafter.

Property	17-4 PH SS as sintered	Aluminium 6061-T6
Ultimate Tensile Strength [MPa]	1050	310
0.2% Yield Strength [MPa]	800	276
Elongation at Break [%]	5	17
Tensile Modulus [GPa]	140	68.9
Density [g/cm³]	7.5 – 7.8*	2.7
Poisson's ratio [/]	0.27**	0.33

Table 1: Material data of Markforged 17-4 PH SS [18] ***and aluminium 6061-T6*** [19]***. *For FE models, a density of 7.8 g/cm³ is chosen. **No Poisson's ratio is given by Markforged and is thus substituted by the value provided in*** [20]***.***

2.2 Lattice design and optimisation procedure

The solid aluminium crank arm model used for reference is a Shimano FC-R450/453, originally mounted to a Giant Anyroad 2 bicycle from 2015. It was mainly chosen as its shape, partly resembling a C-beam, is typical for models produced at high volume and low cost. The crank models for this paper were designed in Autodesk Fusion 360, whereas the lattice structures are generated in nTopology Platform. It allows for fast lattice generation and manipulation as it does not rely on a boundary representation approach for bodies like traditional CAD software suites, but is based on mathematical functions [9]. To determine a suitable lattice structure, the new hollowed steel crank is analysed by replacing its void space with a non-stochastic, beam-based volume lattice and tracing its displacement magnitudes during a typical bicycling loading condition. The performance of each fitting lattice-type available in nTopology Platform is tested separately via the built-in FEA module. The script-like structure of its functionalities allows for quick design changes without repeating tasks like Boolean operations on bodies, meshing, or connecting nodes of solid and beam meshes manually for each design variant. Thus, these tests are exclusively conducted in nTopology Platform. In an initial approach, all lattices exhibit a uniform beam diameter, constant cell size and the lattice orientations coincide with the cartesian coordinate system at hand. The two stiffest lattices showing a weight reduction of at least 80% compared to the negative body, if it were wholly occupied by steel, are retained for further analyses. To gain a marginal weight advantage, their cell sizes are subsequently increased along the longitudinal (Y) crank axis as it is expected not to affect the stiffness drastically. Afterwards, the lattices are rotated about the Y-axis to determine the orientation offering the lowest total compliance. Subsequently, the lattices are partitioned into eight regions, the radii of which are individually optimised for minimal compliance using Altair HyperStudy. As a final verification step, the optimisation results are implemented on both crank arm variants fully discretised by solid elements. Instead of optimising every single beam diameter, as is feasible within Altair OptiStruct, only eight regions have been chosen. Postprocessing becomes very resource-intensive as the number of individual diameter values increases, it is, therefore, preferable to limit them to a sensible amount. In addition, exporting these results for actual manufacturing is only feasible with the third-party software Materialise 3-matic, which is not available to the authors at the moment of writing.

3 Model Description

3.1 CAD Models

3.1.1 Aluminium crank model

The digital replication of the available Shimano crank arm (see Fig. 1) amounts to a weight of 213g, whereas the physical model weighs approximately 225g. For simplification purposes, the exact thread geometry for mounting the pedal as well as the spline joint geometry were neglected. Both are modelled as cylinders causing most of the weight difference between the real and replicated model. The surrogate cylinder diameter for the pedal mount thread is equal to 12.954mm (0.51 inches), i.e., the chosen minor diameter of a 9/16"x20 tpi UN 2B thread common for pedals. The diameter of the cylinder replacing the shaft mount spline is equal to 22mm, i.e., the outer diameter of the shaft geometry. The cylinder centres are 170mm apart – a dimension commonly referred to as the crank length in cycling jargon.

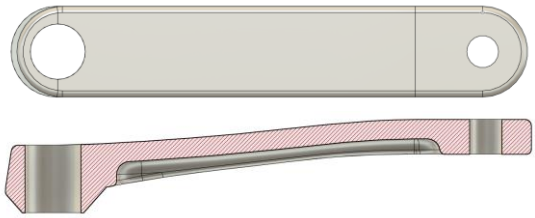

Fig. 1: Front and section view of aluminium crank model with its shaft bore (left side) and pedal bore (right side).

3.1.2 Hollow steel crank model

The new design follows the same dimensions and spacing for functional surfaces as the Shimano model, but is rendered hollow with a wall thickness of 1.6mm (cf. Fig. 2). It is assumed that lower values might compromise manufacturability; thus, a conservative approach is chosen. At the pedal and shaft mounting cylinder surfaces, the thickness is increased to 3mm for strength purposes resulting in a total mass of 276g. A negative body of the inner volume is created via Boolean subtraction in order to generate the volume lattice in nTopology Platform and to track the relative weight reduction. The negative body, weighing 604g, is sectioned into 8 regions for the purpose of generating separate beam sections for the optimisation procedure.

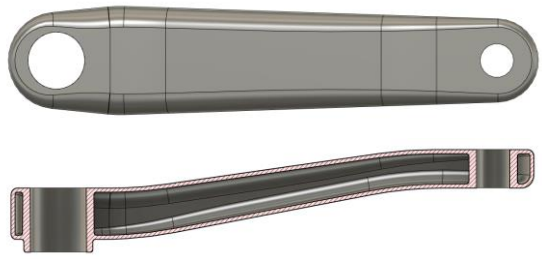

Fig. 2: Front and section view of hollow steel crank model.

3.1.3 Volume lattices

The lattices selected for further analyses consist of re-entrant auxetic and face-centred cubic unit cells. Fig. 3 illustrates the volume lattices, replacing the negative body, with their sectioning and naming scheme after manual alterations were performed. The sectioning is carried out such that the lattices always remains symmetrical about the Y plane, meaning that sections on opposing sides of the lattice exhibit the same beam diameter. Thereby, the number of regions per lattice type to be optimised is kept at a manageable level. Since the lattice's spatial extent along the Z-axis is small compared to its other dimensions, sectioning is only performed along the X and Y axes.

3.2 Load cases

All crank models are loaded according to EN ISO 4210-8 for mountain bikes (see [21]). The forces are induced at a distance of 65mm from the crank's outer surface simulating the cyclist's force acting on the pedal centre, termed point P. The shaft mounting cylinder is rigidly constrained to emulate the shaft connection. Load case 1 defines a force of 1500N acting perpendicularly to the horizontally positioned crank arm. According to the norm, a gear reduction between the smallest chain wheel (front) and the largest sprocket (rear) may be considered, which reduces the applied force proportionally. A gear ratio of 0.8 was chosen in this instance,

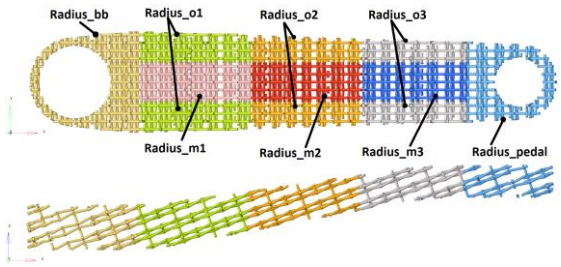

Fig. 3a: Front and top views of re-entrant volume lattice.

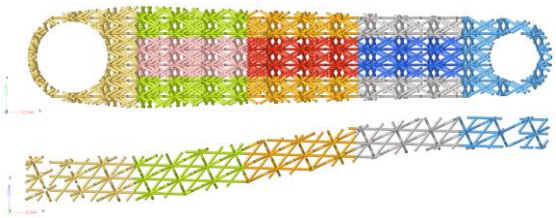

Fig. 3b: Front and top views of face-centred cubic volume lattice.

yielding a force of 1200N. Load cases 2 and 3 specify a force of 1800N acting on the crank without considering any gear reductions, while the crank arm is rotated to angles of 45° and 30° to the horizontal plane, respectively. Although load cases 2 and 3 are intended as fatigue tests with 50.000 load cycles, they are conducted as static tests. Including a fatigue assessment would surpass the scope of this paper, and no fatigue data for 17-4 PH SS produced by this particular manufacturing method is available at the time of writing.

3.3 FEA Models

3.3.1 Model setup in nTopology Platform

In order to create a suitable lattice structure, the negative crank body is replaced by a volume lattice. The hollow crank body is meshed using circa 298.000 second-order tetrahedral elements with an element edge length of 1mm, ensuring the presence of at least two elements across thin walls. The lattice is discretised by second-order one-dimensional beam elements without subdivisions, i.e. all lattice nodes are connected by one single beam element. To determine a suitable lattice configuration, the displacement response of the steel crank body is logged while its lattice properties are altered sequentially. All FE models are carried out as linear static analyses, no nonlinear geometrical or material behaviour is considered. Load case 1 is applied for this initial testing setup. Since the system behaviour remains entirely in the linear domain, its response to the lattice modifications is assumed to be qualitatively similar for the other two load cases and can, in consequence, be extrapolated. In order to connect the beam and solid meshes, all beam element nodes within a distance of 0.5mm to the solid body are coupled.

3.3.2 Model setup in Altair OptiStruct

Using HyperMesh, the aluminium crank model is meshed with 485.000 second-order tetrahedral elements while the hollow steel crank body is discretised by approximately 328.000 second-order tetrahedral elements. Edge lengths range from 0.4mm to 2mm with at least two elements across thin solid walls. Identically to the models in nTopology Platform, the lattice meshes constitute of second-order beam elements with a circular cross-section and no subdivisions. They were exported to HyperMesh/OptiStruct by means of a custom MATLAB script directly converting them to an OptiStruct input file. All calculations are executed as linear static analyses as well. Regarding the boundary condition interfaces, the nodes on the shaft mounting cylinder surface are rigidly constrained (RBE2 connection) at its centre while the node at point P is coupled via an interpolating connection (RBE3), distributing the load to the nodes on the pedal mounting cylinder surface. In the case of the hollow crank models, all beam element nodes within a search distance of 2mm to the crank body are coupled to it by a tie contact. All six degrees of freedom are tied to the movement of the contact master surface on the interior surface of the crank. The slave node adjustment algorithm is set to automatic mode and the contact discretisation type to node-to-surface.

3.4 Numerical optimisation in Altair HyperStudy

To determine the ideal local radii dimensions for the lattices to be analysed, both hollow crank models previously set up in OptiStruct are subjected to an optimisation analysis in Altair HyperStudy. In order to reduce the extent of this paper, only load case 2 is considered for the optimisation since it induces the highest displacement magnitude. For each of the two lattice variations, the beam radii are established as input variables, starting with a uniform radius of 0.5mm and an allowable continuous range of 0.4mm to 1mm. These limits are chosen for ease of manufacturability and to prevent blending of thick beams at their junctions. Four output responses are defined: the maximum displacement magnitude at point P, the total mass, as well as stress values of the solid and beam meshes. To avoid taking outlier stress values into consideration, the mean von Mises stress value plus four times its standard deviation is defined as output response for both lattice and solid bodies. This approach ensures that approximately 99.9936% of all stress values fall inside the specified limit. In this particular case, the outlier values stem from physically not valid stresses caused by the contact interface between the lattice and solid body. A Design of Experiment (DOE) study is conducted using the *Modified Extensible Lattice Sequence* (MELS) method for design space exploration with 50 runs as recommended by HyperStudy. In order to cut calculation time, a response surface using the *Fit Automatically Selected by Training (FAST)* option is then generated to feed into the subsequent optimisation. For the latter, the *Global Response Search Method* (GRSM) is used. The optimisation goal is to minimise the displacement magnitude, while the total mass is limited to 360g. This corresponds to an approximate mass increase of 30% compared to the hollow steel cranks mass without a lattice component. In addition, the stress responses are constrained to the desired upper bound of 320MPa, i.e., 40% of the yield strength as a conservative estimate of the materials' fatigue strength. Values of 400MPa are still deemed acceptable in postprocessing of the final models. For all optimisation constraints, the *Standard Constraint Enforcement* option is active accepting results within 0.5% of the specified limits. The optimised values based on the response surface are verified in OptiStruct as a blend of solid and beam elements before proceeding to the last step.

3.5 Crank models fully discretised by solid elements

In two final analyses, the crank bodies as well as the lattices are completely discretised by solid elements and simulated using Altair OptiStruct in order to check their performance when issues at the contact interfaces between beam and solid elements are eliminated. Following the optimisation step, the optimised beam radii values are applied to the lattices in nTopology Platform, which are then merged with the hollow crank body using a 0.25mm fillet at their boundaries. Surface meshes with 0.25mm element edge length are generated by voxelizing the resulting bodies. The voxel meshes are then smoothed, exported as STL files and remeshed in HyperMesh to reduce the element count while preserving acceptable element quality. Both model variants are subsequently discretised by approximately 3 million second-order tetrahedral elements. The load case and load step setups are identical to the previous models, but element quality checks are disabled as the geometrical complexity hinders high-quality tetrahedral meshing without a substantial time investment.

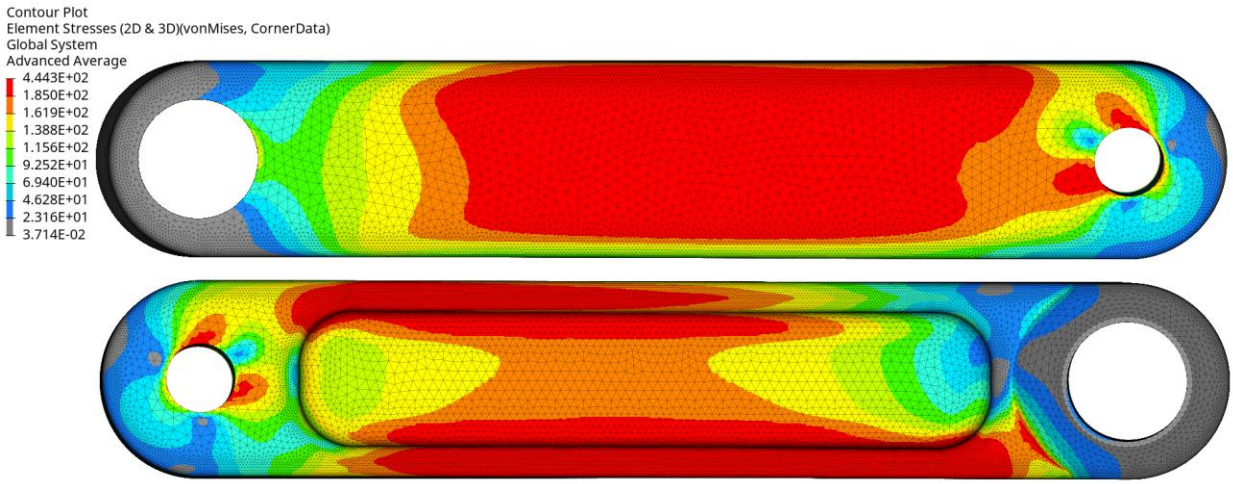

Fig. 4: Von Mises stress distribution of aluminium crank for load condition 2. Red zones show stress values above fatigue strength.

4 Results and discussion

4.1 Solid aluminium crank

The solid aluminium reference crank model calculated in OptiStruct shows the largest displacement magnitude of 7.11mm at point P for load case 2. Significant portions of the crank body show stress values above the fatigue strength of 6061-T6 aluminium, cf. Fig. 4. According to tests conducted in [22], its fatigue stress limit at 50.000 load cycles amounts to approximately 185 MPa. Small regions even surpass its yield strength of 276 MPa.

4.2 Steel crank

4.2.1 Manual lattice alterations

Note: The displacement values of a point on which the remote loads are applied cannot be probed in the software version of nTopology Platform used for this study. The values in the following subsection thus report the maximum displacement magnitudes of the crank body, not of point P.

Starting out the lattice tests with load case 1 and a uniform unit cell with an edge length of 6mm, the re-entrant auxetic and face-centered cubic (FCC) lattices show the least amount of displacement while offering more than 80% weight reduction compared to the solid negative body. This is equivalent to a maximum lattice weight of 120.8g providing a suitable starting point for further weight reduction during the subsequent optimisation process. Both the FCC and re-entrant crank variants show a total deflection of 0.712mm with a weight reduction of 84% and 81%, respectively. Evidently, the completely solid steel crank arm shows the lowest displacement of 0.255mm, whereas the variant without any inner structure exhibits the highest displacement at a value of 0.797mm. Testing shows that increasing the unit cell edge length in multiples of 6mm up to 30mm along the longitudinal axis offers marginal weight savings without significantly compromising the crank stiffness.The approach with 12mm longitudinal edge length is chosen for further procedure as greater values might influence manufacturability. Rotating the lattice about its Y-axis yielded the best results at an angle of -25 degrees for the re-entrant and -20 degrees for the FCC lattice. The displacement magnitude of the FCC crank variant drops to 0.69mm while it is reduced to 0.677mm for the re-entrant variant. In OptiStruct, these values translate to displacement magnitudes of 0.667mm for the re-entrant crank variant and 0.686mm for the FCC crank variant, respectively. The displacement magnitude at the loading point P amounts to 1.57mm for both crank variants.

4.2.2 Numerical optimisation results

The initial and optimised system response values for local beam radii, displacement, stress and mass for both steel crank variants are detailed in Table 2. They are not based on the response surface, but on the verification models under consideration of load case 2 since it causes the greatest displacement values of all three load cases. All the design constraints are satisfied by the optimisation procedure, and although the solid and beam stress values of both models were slightly altered during the procedure, only partial improvements were achieved.

System response	Re-entrant		FCC	
	Initial	Final	Initial	Final
Radius_bb [mm]	0.50	0.47	0.50	0.64
Radius_o1 [mm]	0.50	0.52	0.50	0.54
Radius_o2 [mm]	0.50	0.50	0.50	0.49
Radius_o3 [mm]	0.50	0.43	0.50	0.43
Radius_pedal [mm]	0.50	0.47	0.50	0.49
Radius_m1 [mm]	0.50	0.41	0.50	0.40
Radius_m2 [mm]	0.50	0.40	0.50	0.59
Radius_m3 [mm]	0.50	0.46	0.50	0.40
Displacement [mm]	2.59	2.61	2.57	2.55
Solid stress [MPa]	311.7	313.5	309.8	307.9
Beam stress [MPa]	248.5	261.8	221.7	223.2
Mass [g]	369	357	355	360

Table 2: System response values in load case 2 for both crank variants before and after optimization.

4.2.3 Crank models fully discretised by solid elements

The final displacement magnitudes are slightly lower in comparison to the previous models, amounting to 2.58mm for the re-entrant lattice crank variant and 2.52mm for the FCC lattice crank variant. Locations exhibiting high stress values generally coincide well with the previous results, though the stress concentration issues occurring at the contact interfaces naturally were eliminated. The upper stress limit of 320MPa is locally surpassed, specifically near the pedal and shaft bores models as displayed in Fig. for the crank variant with re-entrant lattice. The high stress regions at the aforementioned locations are slightly less pronounced in the crank variant with the FCC lattice. Stresses in the re-entrant crank variant do not exceed 400MPa except at locations with bad element connections at some beams junctions, which are due to the smoothing and remeshing procedure. Thus, they are not physically valid and can, therefore, be neglected. The FCC variant, on the other hand, displays three regions at beam junctions near the pedal mounting area where the von Mises stress values surpass 400MPa, reaching up to 490MPa as shown in Fig. 6. Both models show stress singularities at the edge of the boundary condition interface of the pedal mounting cylinder, which are physically not valid as well. The total crank weights

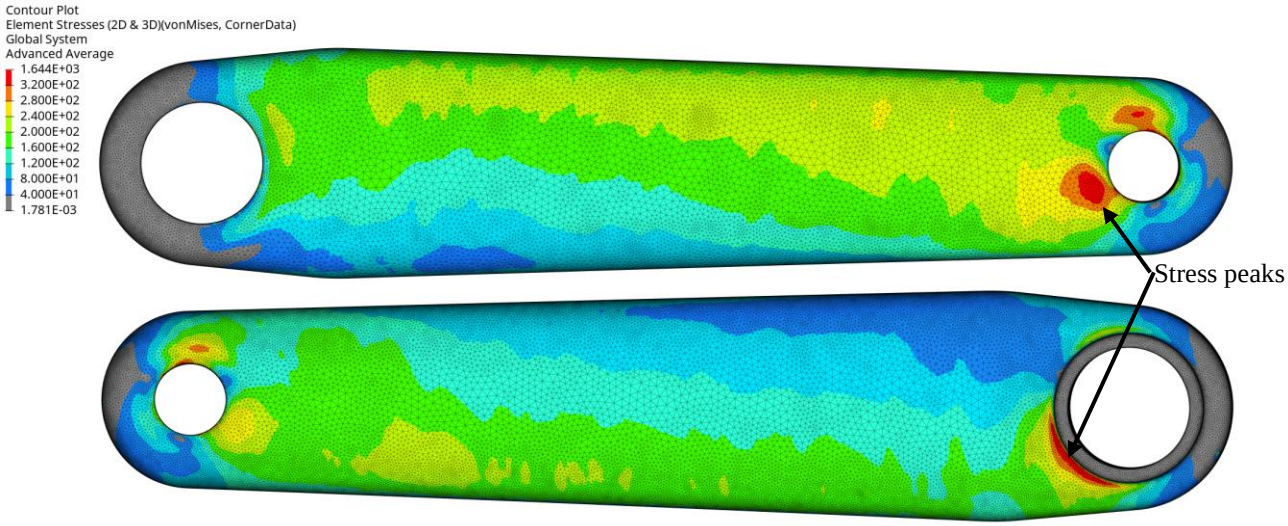

Fig. 5: Von Mises stress distribution of final crank version with re-entrant lattice. Stress values surpassing 320MPa are coloured in red.

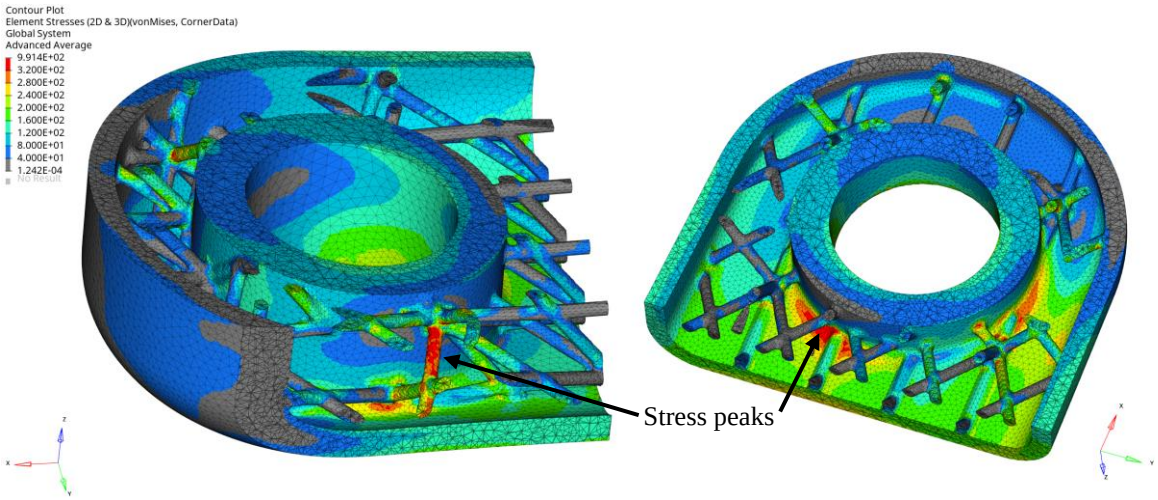

Fig. 6: Von Mises stress peaks of up to 490MPa at pedal bore of final crank variant with FCC lattice. Stress values surpassing 320MPa are coloured in red.

amount to 339g for the re-entrant variant and 341g for the FCC variant. The weight differences to the previous models consisting of solid and beam elements are due to the fact that previously overlapping beam and solid elements are now merged.

4.3 Test prints using FDM

To assess whether the lattice structures are indeed manufacturable using AM, test prints were conducted on an Ultimaker 2 Extended+ FDM machine using the finalised version of the FCC crank variant. Prints using a 0.4mm nozzle and PLA filament showed significant stringing issues and poor beam surface quality at first, especially on their underside. Adjusting the part orientation almost vertically, lowering the print speed, enabling retraction and combing options and, most importantly, reducing the layer height to 0.06mm as well as using a 0.25mm nozzle amongst other minor adjustments netted acceptable results after approximately 80h of printing time as depicted in Fig. 7. Evidently, FDM and ADAM techniques are not entirely comparable and the results of these tests cannot be simply

Fig. 7: FDM test print of final crank variant with FCC lattice, accomplished on an Ultimaker 2 Extended+ using a 0.25mm nozzle and PLA filament.

extrapolated to the Markforged Metal X system. However, the material deposition method is quite similar and the tests might point to difficulties that might occur, especially concerning issues with printing orientation and the need for support structures which are inherently more pronounced in ADAM.

4.4 Discussion

The solid 6061-T6 aluminium crank model was digitally recreated and analysed under EN ISO 4210-8 load conditions. Afterwards, the performance of the redesigned hollow crank made of 17-4 PH steel containing an optimised functionally graded lattice structure was compared to the original one. Analysis of the original crank reveals significant structural flaws; large regions with stresses exceeding the material's fatigue strength with a displacement of 7.11mm at the load application point are formed in the most demanding load case. Some locations also surpass its yield strength and the crank arm would inevitably fail a real test. Following up with analyses of the hollow steel cranks, manual lattice manipulations conducted in nTopology Platform permitted a displacement value decrease of 3.2% for the FCC crank variant and 5.2% for the re-entrant lattice, respectively. The subsequent optimisation step, utilising blends of solid and beam elements in the discretised models, did not succeed in further increasing the total stiffness but adapted the beam diameters to the local stresses. The final models, which were fully discretised by solid elements omitting the contact interfaces and beam elements, are able to slightly improve upon the displacement magnitudes and stress values. Merging the lattice and crank to a single body also reduced the weight of both variants to approximately 340g, undercutting the initial goal of 360g. Displacement values of both variants are further reduced to 2.58mm (re-entrant) and 2.52mm (FCC), respectively. Though the chosen stress limit of 320 MPa could not entirely be met, the crank variant with the re-entrant lattice did not surpass the secondary limit of 400MPa. Small regions in the FCC lattice exhibited stresses of up to 490MPa which might become problematic during a fatigue test. In total, a displacement value decrease of approximately 65% was achieved compared to the aluminium crank, albeit at the detriment of a 59% weight increase.

Prospective topics for future work encompass material property validation, physical printing in metal, testing and exploration of material alternatives like heat-treated stainless steel, titanium, or aluminium to reduce the crank weight. A conceivable alternative to all-metal models may be blends of metal lattices encased in carbon fibre shells such that a continuous fibre can be used. In addition, lattices based on triply periodic minimal surfaces (TPMS) will be analysed in the same context in an upcoming paper. Other potential topics include tapered beams as well as conformal or Voronoi lattices which better adapt to the geometries and can provide more control over local lattice properties. Their basis may be stress vector fields sourced from solid models to influence the exact beam orientation and thicknesses. Additionally, the drive-side crank arm with its direct chainwheel mount, as it is common on today's cranks, and a suitable shaft geometry will be designed for the concluding assembly and tests.

5 Conclusions

This paper shows the practical application of beam-based FGLS on a bicycle crank using a blend of manual adjustments and numerical optimisation methods. Theoretically, the implementation of functionally graded lattice structures in a crank arm in combination with high-performance materials can indeed significantly improve the stiffness of a common bicycle crank. This statement nonetheless holds limited validity. The material properties of 17-4 PH stainless steel produced using ADAM technology are not yet evaluated, and the physical model ultimately has to be tested to support these assertions. Its manufacturability is unexplored and might be hindered by software restrictions of Eiger.io, the preprocessor software provided by Markforged, since it prohibits user control over support structures at the time of writing. Furthermore, a more in-depth exploration of the initial lattice properties, like conformal lattices adapting to a body's surface, blends of different lattice types, cell sizes, or orientations mimicking crystal microstructures like in [23], might have yielded superior results. Future functionalities allowing more control over non-stochastic beam-based lattices to be added to nTopology Platform may provide further potential as well. Though nTopology Platform does offer a utility to create conformal lattices based on CAD faces, its capabilities are not yet sufficient to attain a suitable design with the complex geometry at hand.

References

[1] L. Yang, D. Cormier, H. West, O. Harrysson, and K. Knowlson, “Non-stochastic Ti-6Al-4V foam structures with negative Poisson’s ratio,” *Mater. Sci. Eng. A*, vol. 558, pp. 579–585, 2012, doi: 10.1016/j.msea.2012.08.053.

[2] J. U. Surjadi *et al.*, “Mechanical Metamaterials and Their Engineering Applications,” *Adv. Eng. Mater.*, vol. 21, no. 3, pp. 1–37, 2019, doi: 10.1002/adem.201800864.

[3] W. P. Syam, W. Jianwei, B. Zhao, I. Maskery, W. Elmadih, and R. Leach, “Design and analysis of strut-based lattice structures for vibration isolation,” *Precis. Eng.*, vol. 52, no. May 2017, pp. 494–506, 2018, doi: 10.1016/j.precisioneng.2017.09.010.

[4] K. Davami, M. Mohsenizadeh, M. Munther, T. Palma, A. Beheshti, and K. Momeni, “Dynamic energy absorption characteristics of additivelymanufactured shape-recovering lattice structures,” *Mater. Res. Express*, vol. 6, no. 4, 2019, doi: 10.1088/2053-1591/aaf78c.

[5] R. Mahshid, H. N. Hansen, and K. L. Højbjerre, “Strength analysis and modeling of cellular lattice structures manufactured using selective laser melting for tooling applications,” *Mater. Des.*, vol. 104, pp. 276–283, 2016, doi: 10.1016/j.matdes.2016.05.020.

[6] K. J. Maloney, K. D. Fink, T. A. Schaedler, J. A. Kolodziejska, A. J. Jacobsen, and C. S. Roper, “Multifunctional heat exchangers derived from three-dimensional micro-lattice structures,” *Int. J. Heat Mass Transf.*, vol. 55, no. 9–10, pp. 2486–2493, 2012, doi: 10.1016/j.ijheatmasstransfer.2012.01.011.

[7] M. Helou and S. Kara, “Design, analysis and manufacturing of lattice structures: An overview,” *Int. J. Comput. Integr. Manuf.*, vol. 31, no. 3, pp. 243–261, 2018, doi: 10.1080/0951192X.2017.1407456.

[8] A. Nazir, K. M. Abate, A. Kumar, and J. Y. Jeng, “A state-of-the-art review on types, design, optimization, and additive manufacturing of cellular structures,” *Int. J. Adv. Manuf. Technol.*, vol. 104, no. 9–12, pp. 3489–3510, 2019, doi: 10.1007/s00170-019-04085-3.

[9] G. Allen, “nTopology Modeling Technology,” 2019.

[10] “Printing the future: Cobra Aero rethinks designing for additive manufacturing with nTopology | Association for Unmanned Vehicle Systems International.” https://www.auvsi.org/printing-future-cobra-aero-rethinks-designing-additive-manufacturing-ntopology (accessed Sep. 14, 2020).

[11] M. Vlahinos and R. O. Hara, “Unlocking Advanced Heat Exchanger Design and Simulation with nTop Platform and ANSYS CFX,” 2020.

[12] N/a, “Streamlining additive manufacturing for spinal implants,” 2019. [Online]. Available: http://resources.renishaw.com/en/download/case-study-streamlining-additive-manufacturing-for-spinal-implants--107177.

[13] “S-Works Power Saddle with Mirror.” https://www.specialized.com/us/en/power-saddle-mirror (accessed Jul. 28, 2020).

[14] “Bastion reveals 3D-printed parts for Australia’s 2020 Olympic track campaign | Cycling Smarter.com.”

https://cyclingsmarter.com/bastion-reveals-3d-printed-parts-for-australias-2020-olympic-track-campaign/ (accessed Jul. 28, 2020).

[15] "MOORHUHN 129 - huhncycles." https://huhncycles.com/MOORHUHN-129 (accessed Jul. 28, 2020).

[16] A. Yadollahi, N. Shamsaei, S. Thompson, and A. Elwany, "Fatigue Behavior of 17-4 PH Stainless Steel Fabricated Using Selective Laser Melting," no. August, 2015, doi: 10.13140/RG.2.1.3996.2323.

[17] P. D. Nezhadfar, R. Shrestha, N. Phan, and N. Shamsaei, "Fatigue data for laser beam powder bed fused 17-4 PH stainless steel.pdf." .

[18] Markforged, "Material datasheet 17-4 PH Stainless Steel," 2018.

[19] Matweb, "6061-T6 Matweb," *MatWeb*, pp. 1–2, 2015, [Online]. Available: http://www.matweb.com/search/datasheet.aspx?MatGUID=ff6d4e6d529e4b3d97c77d6538b29693.

[20] Desktop Metal, "17-4 PH Stainless Steel," *Www.Desktopmetal.Com*, p. 1, 2018, [Online]. Available: https://s3.amazonaws.com/desktopmetal/Studio-MDS-17-4-PH-stainless-steel.pdf.

[21] "Cycles - Safety requirements for bicycles - Part 8: Pedal and drive system test methods (ISO 4210-8:2014, Corrected version 2014-11-01)." Comité Européen de Normalisation.

[22] S. Bai, X. Li, Z. Xie, Z. Zhou, and J. Ou, "A wireless fatigue monitoring system utilizing a bio-inspired tree ring data tracking technique," *Sensors (Switzerland)*, vol. 14, no. 3, pp. 4364–4383, 2014, doi: 10.3390/s140304364.

[23] M. S. Pham, C. Liu, I. Todd, and J. Lertthanasarn, "Damage-tolerant architected materials inspired by crystal microstructure," *Nature*, vol. 565, no. 7739, pp. 305–311, 2019, doi: 10.1038/s41586-018-0850-3.